# Chapter 1

# Finite Size and Isotope Shifts

*"If we could only find a supply of atoms with 'point' nuclei we could measure $\Delta E$ and deduce $R$!"*

K. S. Krane

## 1.1 Physical setup: what problem are we solving?

In solving the hydrogen atom one always assumes a point nucleus, $V = -Ze^2/(4\pi\varepsilon_0 r)$. Real nuclei are not points. Lectures 1–2 fixed the charge size from electron scattering: $R_0 \approx 1.2\,\mathrm{fm}\,A^{1/3}$ and a nearly universal skin $t \approx 2.3\,\mathrm{fm}$. The electron wave function penetrates to $r < R$, and inside the charge distribution the potential does *not* diverge as $1/r$. As a first approximation the nucleus may be taken as a uniformly charged sphere of radius $R$. Relative to a point nucleus, $s$-state energies then shift by an amount $\Delta E$ proportional to $Z^4R^2$ (derived below), which is precisely the finite-size correction introduced in Lecture 2.

No sample of point nuclei exists, so absolute finite-size shifts cannot be read off by simple subtraction. What can be measured cleanly is the difference between isotopes: same $Z$, different mass number and slightly different $R$. The isotope shift of $K_\alpha$ X-rays or optical lines then tests nuclear size, and in particular the $R \propto A^{1/3}$ law already suggested by electron scattering [6, 1]. Replacing the electron by a muon amplifies the same effect, because the muon Bohr orbit is about 207 times smaller.

## 1.2 Building the perturbation $H_1$ carefully

### 1.2.1 Point nucleus

For a hydrogen-like ion the electron (charge $-e$) in the field of a *point* nucleus (charge $Ze$) has potential energy

$$U_{\mathrm{point}}(r) = (-e)\cdot\left(\frac{1}{4\pi\varepsilon_0}\frac{Ze}{r}\right) = -\frac{Ze^2}{4\pi\varepsilon_0\, r}. \tag{1.1}$$

The minus sign means attraction: the energy is lowered when the electron approaches the nucleus. As $r \to 0$, $U_{\mathrm{point}} \to -\infty$. That infinite well is unphysical for a real nucleus of finite size.

### 1.2.2 Finite uniform sphere: field and potential

Assume a sphere of radius $R$ with total charge $Ze$ spread uniformly. Gauss's law gives the electric field $E(r)$ (radial, outward for $Z > 0$):

**Outside ($r > R$).** All charge is enclosed, so

$$E(r) = \frac{1}{4\pi\varepsilon_0}\frac{Ze}{r^2}, \qquad V(r) = \frac{1}{4\pi\varepsilon_0}\frac{Ze}{r} \quad (r > R), \tag{1.2}$$

exactly as for a point charge (with $V(\infty) = 0$).

**Inside ($r \le R$).** Only the charge fraction $r^3/R^3$ is enclosed:

$$E(r) = \frac{1}{4\pi\varepsilon_0}\frac{Ze\,r}{R^3}. \tag{1.3}$$

The electrostatic potential is continuous at $r = R$. Integrating inward from the surface,

$$\begin{aligned} V(r) &= V(R) + \int_r^R E(r')\,\mathrm{d}r' \\ &= \frac{1}{4\pi\varepsilon_0}\frac{Ze}{R} + \frac{1}{4\pi\varepsilon_0}\frac{Ze}{R^3}\int_r^R r'\,\mathrm{d}r' \\ &= \frac{1}{4\pi\varepsilon_0}\frac{Ze}{R} + \frac{1}{4\pi\varepsilon_0}\frac{Ze}{R^3}\cdot\frac{1}{2}(R^2 - r^2) \\ &= \frac{1}{4\pi\varepsilon_0}\frac{Ze}{2R}\left(3 - \frac{r^2}{R^2}\right). \end{aligned} \tag{1.4}$$

**Check continuity at $r = R$**

At $r = R$,

$$V(R) = \frac{1}{4\pi\varepsilon_0}\frac{Ze}{2R}(3 - 1) = \frac{1}{4\pi\varepsilon_0}\frac{Ze}{R},$$

which matches the exterior formula. At $r = 0$,

$$V(0) = \frac{1}{4\pi\varepsilon_0}\frac{3Ze}{2R},$$

finite (no singularity).

The electron potential energy is $U = -eV$:

$$U_{\text{finite}}(r) = \begin{cases} -\dfrac{Ze^2}{8\pi\varepsilon_0\,R}\left(3 - \dfrac{r^2}{R^2}\right), & r \le R, \\[2ex] -\dfrac{Ze^2}{4\pi\varepsilon_0\,r}, & r > R. \end{cases} \tag{1.5}$$

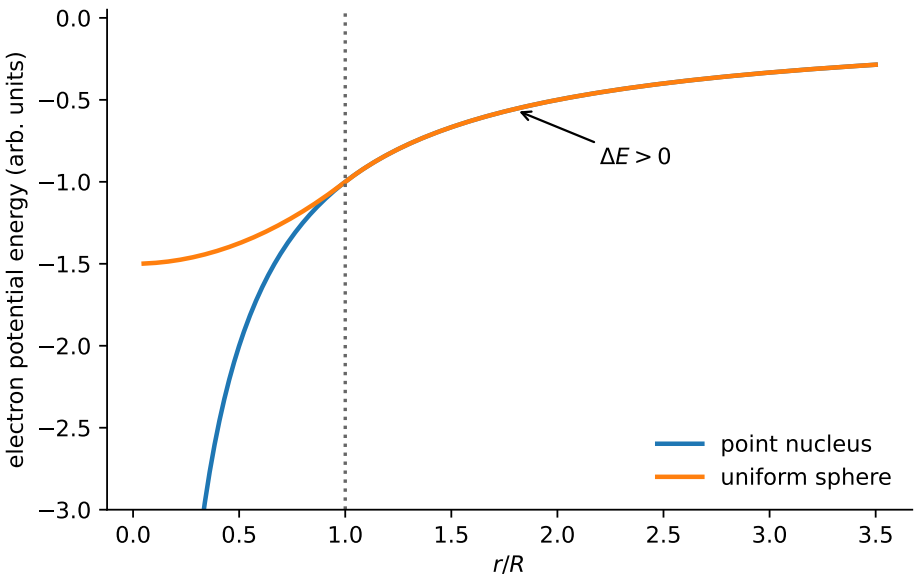


**Figure 1.1:** Electron potential energy for a point nucleus ($U \propto -1/r$, blue) and for a uniformly charged sphere of radius $R$ (red). Outside the nucleus the two curves coincide. Inside, the finite-size well is shallower (less negative) because part of the nuclear charge lies outside the electron's position and attracts less strongly. The dashed lines are schematic $1s$ energies: raising the well raises the bound level from $E_{\text{point}}$ to $E_{\text{finite}}$ by $\Delta E > 0$ (weaker binding).

**Remark**

Compare $U_{\text{finite}}$ and $U_{\text{point}}$ at fixed $r < R$ in Figure 1.1. The finite-size well is *shallower* (less negative) because the electron, when inside the nucleus, does not feel the full Coulomb attraction of all the charge as if it were concentrated at a point. Raising the bottom of the well raises the **bound-state energy** of the electron, here the $1s$ energy $E_{1s}$. In the figure the dashed levels show this shift explicitly:

$$E_{\text{finite}} > E_{\text{point}} \qquad \text{(both negative; } |E_{\text{finite}}| < |E_{\text{point}}|\text{)},$$

so the finite-size correction is $\Delta E = E_{\text{finite}} - E_{\text{point}} > 0$.

**Key idea**

**Reading Figure 1.1.**

- At $r = 0$ the point potential dives to $-\infty$; the finite potential stays finite, $U(0) = -3Ze^2/(8\pi\varepsilon_0 R)$.
- For $0 < r < R$, red lies above blue: less attraction.
- For $r > R$, red = blue (all nuclear charge looks point-like).
- Bound-state energy $E_{1s}$ (dashed) moves up with the well: weaker binding, $\Delta E > 0$.

### 1.2.3 Definition of the perturbation

Write the full Hamiltonian as $H = H_0 + H_1$, where $H_0$ is the usual point-nucleus hydrogen Hamiltonian and

$$H_1(r) \equiv U_{\text{finite}}(r) - U_{\text{point}}(r). \tag{1.6}$$

Outside the nucleus the two potentials agree, so $H_1 = 0$ for $r > R$. Inside,

$$\begin{aligned} H_1(r) &= -\frac{Ze^2}{8\pi\varepsilon_0 R}\left(3 - \frac{r^2}{R^2}\right) - \left(-\frac{Ze^2}{4\pi\varepsilon_0 r}\right) \\ &= -\frac{Ze^2}{8\pi\varepsilon_0 R}\left(3 - \frac{r^2}{R^2}\right) + \frac{Ze^2}{4\pi\varepsilon_0 r}. \end{aligned} \tag{1.7}$$

It is often convenient to factor $k \equiv Ze^2/(4\pi\varepsilon_0)$:

$$H_1(r) = k\left[\frac{1}{r} - \frac{3}{2R} + \frac{r^2}{2R^3}\right], \qquad r \le R. \tag{1.8}$$

**Check $H_1(R) = 0$**

At $r = R$,

$$\frac{1}{R} - \frac{3}{2R} + \frac{1}{2R} = \frac{2 - 3 + 1}{2R} = 0.$$

The perturbation vanishes smoothly at the nuclear surface. If a factor of two is dropped in the Coulomb term, this cancellation fails; that is a common algebraic trap.

**Key idea**

Only the interior region $r < R$ contributes to the energy shift. The entire calculation reduces to an integral of $H_1(r)$ weighted by the electron probability density inside the nucleus.

## 1.3 The $1s$ wave function, step by step

### 1.3.1 Normalised ground state

The hydrogen-like $1s$ wave function is

$$\psi_{1s}(r) = \frac{1}{\sqrt{\pi}}\left(\frac{Z}{a_0}\right)^{3/2} e^{-Zr/a_0}, \tag{1.9}$$

with

$$a_0 = \frac{4\pi\varepsilon_0\hbar^2}{m_e e^2} \approx 0.529\,\text{Å} = 5.29 \times 10^{-11}\,\text{m}. \tag{1.10}$$

**Why these factors?**

- The exponential $e^{-Zr/a_0}$ is the solution of the radial Schrödinger equation for $n = 1$, $\ell = 0$. Larger $Z$ pulls the cloud inward (effective Bohr radius $a_0/Z$).

- The prefactor is fixed by normalisation $\int |\psi|^2 \, \mathrm{d}^3 r = 1$. For a purely radial function, $\int_0^\infty 4\pi r^2 |\psi|^2 \, \mathrm{d}r = 1$.

**Density at the origin.** Set $r = 0$:

$$\psi_{1s}(0) = \frac{1}{\sqrt{\pi}} \left( \frac{Z}{a_0} \right)^{3/2}, \qquad |\psi_{1s}(0)|^2 = \frac{Z^3}{\pi a_0^3}. \tag{1.11}$$

The $Z^3$ dependence is crucial: heavier nuclei (larger $Z$) pack far more electron density near $r = 0$, so finite-size shifts grow rapidly with $Z$.

**Caution**

$\psi_{1s}$ itself is proportional to $Z^{3/2}$, not $Z^3$. The quantity $Z^3/(\pi a_0^3)$ is $|\psi(0)|^2$, the probability density. Mixing the two is a frequent source of wrong powers of $Z$ in $\Delta E$.

### 1.3.2 First-order perturbation theory (what the formula means)

If the unperturbed eigenproblem is $H_0 \psi_n = E_n^{(0)} \psi_n$ and we add a small $H_1$, the first-order energy correction is

$$\Delta E_n = \langle \psi_n | H_1 | \psi_n \rangle = \int \psi_n^* \, H_1 \, \psi_n \, \mathrm{d}^3 r. \tag{1.12}$$

For the real $1s$ wave function this is simply the expectation value of $H_1$ in the unperturbed ground state:

$$\Delta E = \int |\psi_{1s}(r)|^2 H_1(r) \, \mathrm{d}^3 r. \tag{1.13}$$

**Physical reading:** average the extra potential energy $H_1$ with the probability density of finding the electron at each point. Since $H_1 = 0$ outside the nucleus, only the nuclear ball contributes.

## 1.4 Evaluating $\Delta E$: full algebraic development

### 1.4.1 Write the integral in spherical coordinates

Because $|\psi_{1s}|^2$ and $H_1$ depend only on $r$,

$$\mathrm{d}^3 r = 4\pi r^2 \, \mathrm{d}r, \tag{1.14}$$

and

$$\Delta E = \int_0^R \underbrace{\frac{Z^3}{\pi a_0^3} e^{-2Zr/a_0}}_{|\psi_{1s}(r)|^2} H_1(r) \, 4\pi r^2 \, \mathrm{d}r. \tag{1.15}$$

(The factor $e^{-2Zr/a_0}$ comes from $|e^{-Zr/a_0}|^2 = e^{-2Zr/a_0}$.)

### 1.4.2 Approximation: the exponential is almost 1

We must integrate only up to $r = R$. Compare length scales:

| Quantity | Typical size | Comment |
|---|---|---|
| Nuclear radius $R$ | $\sim 1 - -7\,\mathrm{fm}$ | few fm |
| Bohr radius $a_0$ | $5.29 \times 10^{-11}\,\mathrm{m}$ | atomic scale |
| Ratio $R/a_0$ | $\sim 2 \times 10^{-5}$ | extremely small |

For any $r \le R$,

$$\frac{2Zr}{a_0} \le \frac{2ZR}{a_0} \sim 2Z \times 10^{-5}. \tag{1.16}$$

Even for uranium ($Z = 92$),

$$\frac{2ZR}{a_0} \approx \frac{2(92)(7.4\,\mathrm{fm})}{5.29 \times 10^4\,\mathrm{fm}} \approx 2.6 \times 10^{-2} \ll 1. \tag{1.17}$$

Taylor expand:

$$e^{-2Zr/a_0} = 1 - \frac{2Zr}{a_0} + \cdots \approx 1, \tag{1.18}$$

with a relative error below a few percent even for the heaviest electronic ions, and much smaller for moderate $Z$. For high $Z$, relativistic Dirac wave functions are nevertheless required for precision work. Therefore, to an excellent approximation,

$$\Delta E \approx |\psi_{1s}(0)|^2 \int_0^R H_1(r)\, 4\pi r^2\, \mathrm{d}r = |\psi_{1s}(0)|^2 \int_{r<R} H_1\, \mathrm{d}^3 r. \tag{1.19}$$

**Key idea**

Because the nucleus is a speck on the atomic scale, the electron density hardly varies across it. Pull $|\psi(0)|^2$ out of the integral; only the volume integral of $H_1$ remains.

### 1.4.3 Volume integral of $H_1$ (line by line)

Start from Equation (1.8):

$$H_1(r) = k\left(\frac{1}{r} - \frac{3}{2R} + \frac{r^2}{2R^3}\right), \qquad k = \frac{Ze^2}{4\pi\varepsilon_0}. \tag{1.20}$$

Then

$$\begin{aligned} I &\equiv \int_{r<R} H_1\, \mathrm{d}^3 r = \int_0^R H_1(r)\, 4\pi r^2\, \mathrm{d}r \\ &= 4\pi k \int_0^R \left(r - \frac{3r^2}{2R} + \frac{r^4}{2R^3}\right) \mathrm{d}r. \end{aligned} \tag{1.21}$$

Integrate term by term:

$$\int_0^R r\,\mathrm{d}r = \frac{R^2}{2}, \tag{1.22}$$

$$\int_0^R \frac{3r^2}{2R}\,\mathrm{d}r = \frac{3}{2R}\cdot\frac{R^3}{3} = \frac{R^2}{2}, \tag{1.23}$$

$$\int_0^R \frac{r^4}{2R^3}\,\mathrm{d}r = \frac{1}{2R^3}\cdot\frac{R^5}{5} = \frac{R^2}{10}. \tag{1.24}$$

The first two contributions cancel:

$$\frac{R^2}{2} - \frac{R^2}{2} + \frac{R^2}{10} = \frac{R^2}{10}. \tag{1.25}$$

Therefore

$$I = 4\pi k\cdot\frac{R^2}{10} = \frac{2\pi}{5}\,k\,R^2 = \frac{2\pi}{5}\frac{Ze^2}{4\pi\varepsilon_0}R^2 = \frac{Ze^2R^2}{10\,\varepsilon_0}. \tag{1.26}$$

**Why the cancellation?**

The $1/r$ and constant pieces of $H_1$ rearrange the Coulomb singularity into a finite well. Their weighted integrals over the ball cancel, leaving only the $r^2$ piece of the interior potential, which produces the factor $R^2/10$. That is why $\Delta E \propto R^2$, not $R^3$: after cancellation one power of $R$ is lost relative to a naive volume estimate.

### 1.4.4 Assemble $\Delta E$

$$\begin{aligned}\Delta E &= |\psi_{1s}(0)|^2\, I = \frac{Z^3}{\pi a_0^3}\cdot\frac{2\pi}{5}\cdot\frac{Ze^2}{4\pi\varepsilon_0}R^2\\ &= \frac{Z^3}{\pi a_0^3}\cdot\frac{Ze^2R^2}{10\,\varepsilon_0}\cdot\frac{2\pi}{2\pi}\\ &= \frac{Z^4e^2R^2}{10\pi\,\varepsilon_0\,a_0^3}.\end{aligned} \tag{1.27}$$

**Final formula: $1s$ finite-size shift (uniform sphere)**

$$\boxed{\Delta E_{1s} = \frac{Z^4e^2R^2}{10\pi\,\varepsilon_0\,a_0^3} > 0}$$

**How to read the powers.**

- $Z^4 = Z\cdot Z^3$: one $Z$ from the Coulomb strength $Ze^2$, and $Z^3$ from $|\psi(0)|^2$.
- $R^2$: residual after the integral cancellation discussed above.
- $1/a_0^3$: denser electron cloud for smaller Bohr radius.
- Positive sign: the well is shallower, so the level moves *up* (less bound).

**Example: scaling with $Z$ and $R$**

Compare hydrogen ($Z = 1$, $R \sim 1\,\mathrm{fm}$) with mercury ($Z = 80$, $R \sim 7\,\mathrm{fm}$):

$$\frac{\Delta E(\mathrm{Hg})}{\Delta E(\mathrm{H})} \sim 80^4 \times 7^2 \approx 4.1 \times 10^7 \times 49 \approx 2 \times 10^9.$$

Hydrogen's shift is $\sim 10^{-10}$ of $|E_{1s}|$; mercury's absolute shift is still only $\sim 0.1\,\mathrm{eV}$, but that is measurable against a $K_\alpha$ energy of $\sim 100\,\mathrm{keV}$.

### 1.4.5 Link to the mean-square radius

For a general spherical charge density (not necessarily uniform), the leading result follows most cleanly in momentum space. Normalise its form factor by

$$F(\boldsymbol{q}) = \frac{1}{Ze}\int \rho_{\mathrm{ch}}(\boldsymbol{r})\, e^{i\boldsymbol{q}\cdot\boldsymbol{r}/\hbar}\,\mathrm{d}^3r = 1 - \frac{q^2\langle r^2\rangle_{\mathrm{ch}}}{6\hbar^2} + O(q^4).$$

The Coulomb kernel is proportional to $\hbar^2/q^2$. Subtracting the point source cancels the pole:

$$\begin{aligned}\delta U(\boldsymbol{q}) &= -\frac{Ze^2\hbar^2}{\varepsilon_0 q^2}\left[F(\boldsymbol{q}) - 1\right] \\ &= \frac{Ze^2}{6\varepsilon_0}\langle r^2\rangle_{\mathrm{ch}} + O(q^2).\end{aligned} \tag{1.28}$$

A constant in momentum space is a contact interaction in position space,

$$\delta U(\boldsymbol{r}) = \frac{2\pi}{3}\frac{Ze^2}{4\pi\varepsilon_0}\,\langle r^2\rangle_{\mathrm{ch}}\,\delta^{(3)}(\boldsymbol{r}) + \text{higher moments.} \tag{1.29}$$

Taking its expectation value gives

$$\begin{aligned}\Delta E_{1s} &= |\psi_{1s}(0)|^2 \int \left[U_{\mathrm{finite}}(\boldsymbol{r}) - U_{\mathrm{point}}(\boldsymbol{r})\right]\mathrm{d}^3r \\ &= \frac{2\pi}{3}\frac{Ze^2}{4\pi\varepsilon_0}\langle r^2\rangle_{\mathrm{ch}}|\psi_{1s}(0)|^2,\end{aligned} \tag{1.30}$$

where omitted terms contain higher nuclear moments and derivatives of the electronic density. For a uniform sphere,

$$\langle r^2\rangle = \frac{\int_0^R r^2\cdot 4\pi r^2\,\mathrm{d}r}{\frac{4}{3}\pi R^3} = \frac{3}{5}R^2. \tag{1.31}$$

Inserting this into Equation (1.30) recovers Equation (1.27):

$$\frac{2\pi}{3}\,k\cdot\frac{3}{5}R^2\cdot\frac{Z^3}{\pi a_0^3} = \frac{2\pi}{5}\,kR^2\cdot\frac{Z^3}{\pi a_0^3} = \frac{Z^4e^2R^2}{10\pi\varepsilon_0 a_0^3}. \tag{1.32}$$

So the uniform-sphere calculation is a special case of a more general theorem: the leading shift measures $\langle r^2\rangle_{\mathrm{ch}}$.

Writing $E_{1s}^{\mathrm{point}}$ for the unperturbed energy,

$$E_{1s} = E_{1s}^{\mathrm{point}} + \Delta E_{1s}. \tag{1.33}$$

## 1.5 $K_\alpha$ X-rays: from levels to a measurable line

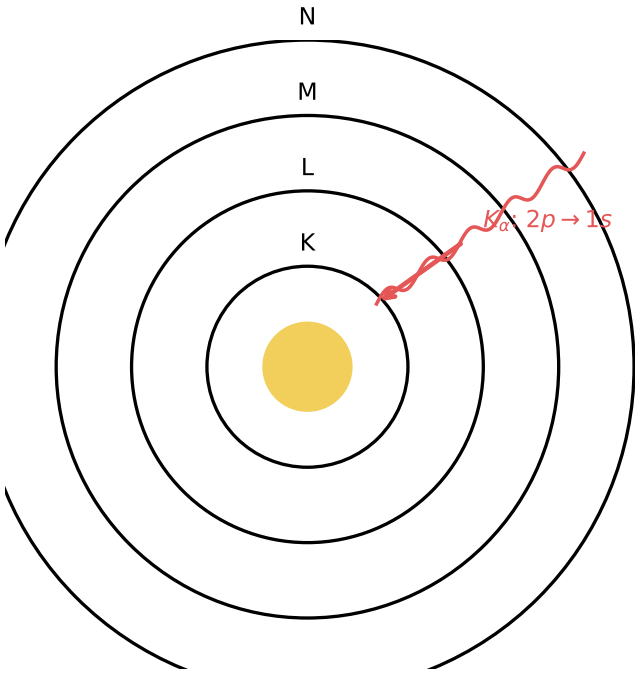


**Figure 1.2:** Atomic shells. A vacancy in the $K$ shell ($1s$) is filled from a higher shell, emitting an X-ray. $K_\alpha$ corresponds mainly to $2p \to 1s$; $K_\beta$ involves higher initial levels.

### 1.5.1 What is measured?

If a $1s$ electron is removed, an electron from a higher shell can drop into the vacancy. The energy difference is emitted as a characteristic X-ray (Figure 1.2). The $K_\alpha$ complex is dominated by $2p \to 1s$ transitions.

**Historical note: Henry Moseley (1887–1915)**

**Henry Gwyn Jeffreys Moseley** showed (1913–1914) that characteristic X-ray frequencies scale as $(Z-1)^2$, establishing $Z$ as the true ordering parameter of the elements. That is why $K_\alpha$ energies are such a clean probe of nuclear charge and, through isotope shifts, of nuclear size.

### 1.5.2 Point-nucleus level energies

For a hydrogen-like ion,

$$E_n^{\text{point}} = -\frac{m_e Z^2 e^4}{8\varepsilon_0^2 h^2 n^2} = -\frac{Z^2}{n^2}\,\text{Ry}, \qquad \text{Ry} \approx 13.6\,\text{eV}. \tag{1.34}$$

Thus

$$E_{1s}^{\text{point}} = -Z^2\,\text{Ry}, \qquad E_2^{\text{point}} = -\frac{Z^2}{4}\,\text{Ry} \quad (\text{includes } 2p). \tag{1.35}$$

**Photon energy for $2p \to 1s$.** The electron falls from a less-bound level to a more-bound level. The photon energy is

$$\begin{aligned} E_{K_\alpha}^{\text{point}} &= E_2^{\text{point}} - E_{1s}^{\text{point}} \\ &= \left(-\frac{Z^2}{4} + Z^2\right)\text{Ry} = \frac{3}{4}\,Z^2\,\text{Ry}. \end{aligned} \tag{1.36}$$

(For real atoms, screening replaces $Z$ by $\approx Z - 1$, as in Moseley's law; the structure of the finite-size argument is unchanged.)

### 1.5.3 How $\Delta E_{1s}$ changes $K_\alpha$

In non-relativistic theory, $p$-state wave functions vanish at $r = 0$, so their finite-size shifts are much smaller than that of $1s$. Keeping only $\Delta E_{1s}$,

$$\begin{aligned} E_{K_\alpha} &= E_2^{\text{point}} - (E_{1s}^{\text{point}} + \Delta E_{1s}) \\ &= (E_2^{\text{point}} - E_{1s}^{\text{point}}) - \Delta E_{1s} \\ &= E_{K_\alpha}^{\text{point}} - \Delta E_{1s}. \end{aligned} \tag{1.37}$$

**Sign: why $K_\alpha$ softens**

- Finite size raises $E_{1s}$ (makes it less negative).
- $E_2$ is almost unchanged.
- The gap $E_2 - E_{1s}$ therefore shrinks.
- The emitted X-ray has slightly lower energy.

**Key idea**

$$E_{K_\alpha} = E_{K_\alpha}^{\text{point}} - \frac{Z^4 e^2 R^2}{10\pi\,\varepsilon_0\,a_0^3}.$$

Larger $R \Rightarrow$ smaller $E_{K_\alpha}$.

## 1.6 Isotope shifts: cancelling everything except $R$

### 1.6.1 Why isotopes?

Two isotopes of the same element have:

- the *same* $Z$ (same Coulomb strength, same electronic structure to an excellent approximation);
- *different* $A$, hence different nuclear radii $R(A)$.

The dominant point-nucleus pieces cancel in a difference, but a measured isotope shift is not a pure radius observable without atomic-structure corrections.

**Field shift versus mass shift**

For a transition $i$, the leading isotope shift is

$$\delta\nu_i^{A,A'} = K_{i,\mathrm{MS}}\left(\frac{1}{A} - \frac{1}{A'}\right) + F_i\,\delta\langle r^2\rangle^{A,A'} + \cdots .$$

The first term is the normal plus specific *mass shift* (nuclear recoil and correlated electron motion); the second is the *field shift* caused by the changed charge distribution. In heavy atoms the field shift often dominates, but extracting a radius still requires calculated $K_{i,\mathrm{MS}}$ and $F_i$. Electron screening, relativistic wave functions, nuclear deformation, and higher moments also matter. In Dirac theory even $p_{1/2}$ states have nonzero nuclear overlap, so the claim that every $p$ shift vanishes is only a non-relativistic leading-order statement [6, 2].

### 1.6.2 Algebra for two isotopes

Let the reference isotope have mass number $A_0$ and radius $R_0$, and another isotope have $A$ and $R$. Then

$$E_{K_\alpha}(A_0) = E_{K_\alpha}^{\mathrm{point}} - CR_0^2, \tag{1.38}$$
$$E_{K_\alpha}(A) = E_{K_\alpha}^{\mathrm{point}} - CR^2, \tag{1.39}$$

where we abbreviated the positive constant

$$C \equiv \frac{Z^4e^2}{10\pi\,\varepsilon_0\,a_0^3}. \tag{1.40}$$

Subtract:

$$\begin{aligned}\Delta E_{K_\alpha} &\equiv E_{K_\alpha}(A) - E_{K_\alpha}(A_0)\\ &= (E_{K_\alpha}^{\mathrm{point}} - CR^2) - (E_{K_\alpha}^{\mathrm{point}} - CR_0^2)\\ &= C(R_0^2 - R^2).\end{aligned} \tag{1.41}$$

**Interpretation.** If the second isotope is heavier, typically $R > R_0$, so $R_0^2 - R^2 < 0$ and $\Delta E_{K_\alpha} < 0$. The heavier isotope's $K_\alpha$ line lies at slightly lower energy. Experimental plots often display $-\Delta E_{K_\alpha}$ (a positive quantity that grows with $A$).

### 1.6.3 Insert $R_0 = 1.2\,\mathrm{fm}\,A^{1/3}$

Electron-scattering systematics give the half-density radius [1]

$$R = R_0 = 1.2\,\mathrm{fm}\times A^{1/3} \quad\Rightarrow\quad R^2 = (1.2\,\mathrm{fm})^2\,A^{2/3}. \tag{1.42}$$

Then

$$\Delta E_{K_\alpha} = C\,(1.2\,\mathrm{fm})^2(A_0^{2/3} - A^{2/3}) = \frac{Z^4e^2}{10\pi\,\varepsilon_0\,a_0^3}(1.2\,\mathrm{fm})^2(A_0^{2/3} - A^{2/3}). \tag{1.43}$$

Equivalently,

$$-\Delta E_{K_\alpha} = C\,(1.2\,\mathrm{fm})^2(A^{2/3} - A_0^{2/3}). \tag{1.44}$$

**What to plot**

Fix a reference isotope $A_0$. For each other isotope $A$, compute $-\Delta E_{K_\alpha}$ and plot it against $A^{2/3}$.

- **If the points fall on a straight line**, the data support $R \propto A^{1/3}$.
- **The slope** equals $C \times (1.2\,\mathrm{fm})^2$ if the $R_0$ law holds; a measured slope is a consistency check on that same coefficient.

**Takeaway**

Experimental checklist:

1. Measure $E_{K_\alpha}$ for several isotopes of one element.
2. Form shifts relative to a reference isotope.
3. Plot $-\Delta E$ versus $A^{2/3}$.
4. Linearity $\Rightarrow R \propto A^{1/3}$; slope checks $R_0 = 1.2\,\mathrm{fm}\,A^{1/3}$ from form-factor data [1].

### 1.6.4 Mercury data

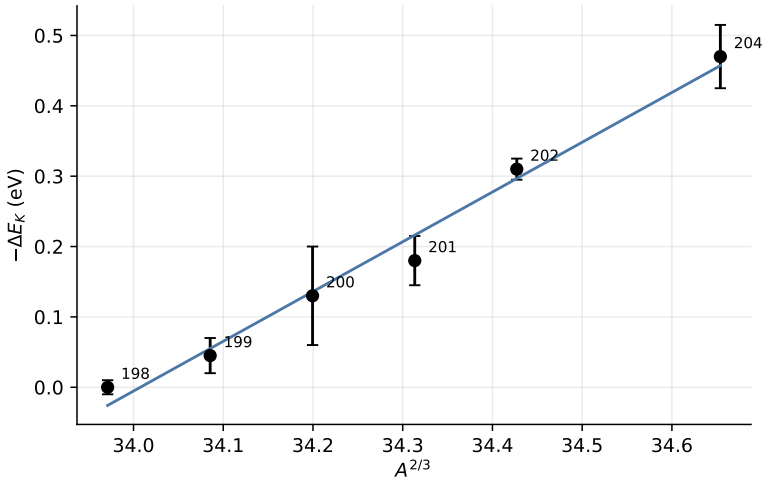


**Figure 1.3:** $K_\alpha$ isotope shifts in mercury ($Z = 80$), plotted as $-\Delta E$ versus $A^{2/3}$ relative to $^{198}$Hg. Even and odd isotopes lie on nearly straight lines, as expected if $R \propto A^{1/3}$. Data-redrawn from Krane, Fig. 3.6, p. 52 (Lee et al., Phys. Rev. C **17**, 1859 (1978)).

Mercury ($Z = 80$) has several stable isotopes near $A \sim 200$. Figure 1.3 plots $-\Delta E$ against $A^{2/3}$ with $^{198}$Hg as reference. The near-linearity is the experimental signature of $R \propto A^{1/3}$. Small odd–even staggering reflects pairing and slight deformation beyond the ideal spherical model.

**Example: how small is the shift?**

For mercury,

$$E_{K_\alpha} \sim 100\,\text{keV} = 10^5\,\text{eV}, \qquad |\Delta E| \sim 0.1\,\text{eV} \text{ between nearby isotopes.}$$

The fractional change is

$$\frac{|\Delta E|}{E_{K_\alpha}} \sim 10^{-6}.$$

That is one part per million: tiny, but accessible to modern precision X-ray spectroscopy. The slope of the line, together with many other experiments, gives the standard $r_0 \approx 1.2\,\text{fm}$.

## 1.7 Muonic atoms: the same maths with a heavy lepton

Electronic shifts are parts per million. Nature provides a louder version of the same calculation: replace the electron by a muon.

### 1.7.1 Muon basics

The muon $\mu^-$ has charge $-e$ and mass

$$m_\mu \approx 207\, m_e. \tag{1.45}$$

Lifetime $\tau_\mu \approx 2.2\,\mu\text{s}$ (rest frame), long enough to be captured into atomic orbits and emit X-rays before decaying ($\mu^- \to e^- \bar{\nu}_e \nu_\mu$).

**Historical note: Carl D. Anderson (1905–1991)**

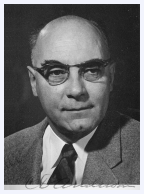

**Carl David Anderson** discovered the positron (1932) and the muon in cosmic rays (1936, with Neddermeyer). The muon was first mistaken for Yukawa's meson; it is in fact a heavy lepton. Anderson's particle is the probe behind modern muonic-atom determinations of nuclear charge radii.

### 1.7.2 How the Bohr radius scales

The Bohr radius comes from balancing Coulomb attraction against kinetic energy. With reduced mass $\mu$ of the orbiting lepton and the nucleus,

$$a_\mu = \frac{4\pi\varepsilon_0\,\hbar^2}{\mu e^2} = a_\text{B}\,\frac{m_e}{\mu}. \tag{1.46}$$

For an electron on a heavy nucleus, $\mu \approx m_e$ and $a \approx a_\text{B}$. For a muon, $\mu \approx m_\mu$ (still $\ll m_\text{nucleus}$), so

$$a_\mu = a_0\,\frac{m_e}{m_\mu} \approx \frac{a_0}{207}. \tag{1.47}$$

**Caution**

The mass ratio is $\approx 207$, not 27. Hence $a_\mu = a_0/207$. Using 27 underestimates how tightly the muon is bound by almost an order of magnitude in linear size.

### 1.7.3 How $\Delta E$ scales for a muon

Repeat Equation (1.27) with $a_0 \to a_\mu$ and $m_e \to m_\mu$ in the wave function. The structure is unchanged:

$$\Delta E^{(\mu)} = \frac{Z^4 e^2 R^2}{10\pi\,\varepsilon_0\, a_\mu^3}. \tag{1.48}$$

Compared with the electronic shift,

$$\frac{\Delta E^{(\mu)}}{\Delta E^{(e)}} = \left(\frac{a_0}{a_\mu}\right)^3 = \left(\frac{m_\mu}{m_e}\right)^3 \approx 207^3 \approx 8.9 \times 10^6. \tag{1.49}$$

So muonic finite-size shifts are roughly *ten million times* larger in the naive scaling (before accounting for the fact that for heavy nuclei the muon orbit is so small that the constant-$\psi$ approximation and non-relativistic theory both need upgrading).

**Example: muon $K$-shell size in lead**

Electron $K$ radius $\sim a_0/Z$. Muon $K$ radius $\sim a_\mu/Z = a_0/(207\,Z)$. For lead ($Z = 82$),

$$\frac{a_\mu}{Z} \approx \frac{0.529\ \text{Å}}{207 \times 82} \approx 3\,\text{fm},$$

comparable to the nuclear radius. The muon wave function overlaps the nuclear charge distribution strongly; precision $\langle r^2 \rangle$ follows from measured muonic X-ray energies.

**Key idea**

Same formulae, different mass: muonic atoms turn a parts-per-million electronic effect into a large, accurately measurable shift, at the price of a more careful (often relativistic, numerical) treatment for heavy $Z$.

**Remark**

For heavy nuclei one no longer pulls $|\psi(0)|^2$ out as a constant: the muon $1s$ state varies over nuclear dimensions. One then solves the Dirac equation in the electrostatic potential of a realistic $\rho(r)$ and adjusts $\langle r^2 \rangle$ (or a full density model) to match the observed transitions. The conceptual origin of the shift is still the same $H_1$ we built in Section 1.2.

## 1.8 Worked summary of the mathematics

**One-page derivation map**

1. $U_{\text{point}} = -\dfrac{Ze^2}{4\pi\varepsilon_0 r}$.
2. Uniform sphere $\Rightarrow U_{\text{finite}} = -\dfrac{Ze^2}{8\pi\varepsilon_0 R}(3 - r^2/R^2)$ for $r \le R$.
3. $H_1 = U_{\text{finite}} - U_{\text{point}}$ (zero outside).
4. $\Delta E = \int |\psi_{1s}|^2 H_1 \, \mathrm{d}^3 r$.
5. $e^{-2Zr/a_0} \approx 1$ on $r \le R$ because $R \ll a_0$.
6. $\Delta E \approx |\psi(0)|^2 \int H_1 \, \mathrm{d}^3 r$.
7. $\int H_1 \, \mathrm{d}^3 r = \dfrac{2\pi}{5} k R^2$ after cancellation of two terms in the radial integral.
8. $|\psi(0)|^2 = Z^3/(\pi a_0^3) \Rightarrow \Delta E = \dfrac{Z^4 e^2 R^2}{10\pi\varepsilon_0 a_0^3}$.
9. $E_{K_\alpha} = E_{K_\alpha}^{\text{point}} - \Delta E$.
10. Isotope difference $\propto (R_0^2 - R^2)$; with $R = 1.2\,\text{fm}\, A^{1/3}$, plot vs $A^{2/3}$.
11. Muon: replace $a_0 \to a_0/207$; shift grows as $207^3$.

## 1.9 Three experimental routes to nuclear size

1. **Electron scattering** (Lectures 1–2). Maps $F(q)$ and $\rho_p(r)$; yields $R_0 = 1.2\,\text{fm}\, A^{1/3}$ and $a = 0.52\,\text{fm} \pm 0.01\,\text{fm}$ [1].
2. **Electronic $K_\alpha$ isotope shifts** (this lecture). $\Delta E_{1s} = Z^4 e^2 R^2/(10\pi\varepsilon_0 a_0^3)$ softens $K_\alpha$; differences test $A^{1/3}$ via linearity in $A^{2/3}$.
3. **Muonic atoms**. Same maths with $a_\mu = a_0/207$; much larger shifts and precise $\langle r^2 \rangle_{\text{ch}}$.

**Takeaway**

The algebra is lengthy, but the physics is simple: a finite nucleus softens the Coulomb singularity, raises $s$-state energies by an amount $\propto Z^4 R^2$, and that shift is visible in X-rays once you compare isotopes or switch to muons. The same $R_0 = 1.2\,\text{fm}\, A^{1/3}$ that appears in electron scattering [1] reappears in the slope of the isotope-shift plot.

**Next.** Lecture 4 leaves size for *energy*: binding energy, the $B/A$ curve, and the liquid-drop SEMF. Lecture 5 then turns the same mass formula into mass parabolas and $\beta$ stability.

## 1.10 Deeper physics: comparing size probes

Lectures 1–3 measure nuclear size three ways. The results agree at the percent level only when each method quotes a carefully defined moment of $\rho_{\text{ch}}$ [6, 1, 2].

### 1.10.1 Electron scattering vs atomic shifts

| Probe | What is measured | Sensitivity |
|---|---|---|
| Elastic $e^-$ scattering | $\lvert F(q)\rvert^2 \to \rho_{\mathrm{ch}}(r)$ | Full radial profile; model-dependent at large $q$ |
| Electronic $K_\alpha$ / optical isotope shift | $\Delta\langle r^2\rangle$ between isotopes | Relative radii; absolute scale needs calibration |
| Muonic atoms | Large finite-size shift $\propto m_\mu^3$ | Absolute $\langle r^2\rangle_{\mathrm{ch}}$ for many $Z$ |

Muonic $1s$ levels are far more sensitive than electronic ones because the Bohr radius scales as $1/m$: $m_\mu/m_e \approx 207$ compresses the orbit by the same factor and boosts the overlap with the nucleus by $\sim 207^3$. That is why muonic X-rays became a precision tool for charge radii once muon beams were available [2, 6].

### 1.10.2 Mean-square radius as the universal intermediate

All three methods ultimately quote moments of $\rho_{\mathrm{ch}}$. For a uniform sphere of radius $R$,

$$\langle r^2\rangle = \tfrac{3}{5}R^2, \tag{1.50}$$

so $R_{\mathrm{eq}} = \sqrt{5/3}\,\langle r^2\rangle^{1/2}$. Isotope-shift formulae depend on $\delta\langle r^2\rangle$, not on a model-dependent surface thickness. Electron scattering at low $q$ measures the same $\langle r^2\rangle$ from the form-factor curvature (Lecture 1). Agreement among methods is a major empirical success of nuclear charge-density physics.

**Order of magnitude for the $1s$ shift**

For $Z \sim 80$ and $R \sim 7\,\mathrm{fm}$, the electronic finite-size correction to the $1s$ level is only of order eV–keV on a keV–MeV scale, yet modern X-ray and laser spectroscopy resolve isotope differences cleanly. The same algebra with $m \to m_\mu$ yields keV to MeV shifts: muonic spectroscopy is a nuclear, not atomic, measurement in disguise [6].

**Key idea**

**Absolute shift vs isotope difference.** The absolute finite-size correction $\Delta E(A,Z)$ is entangled with atomic-structure uncertainties. Differences $\Delta E(A,Z) - \Delta E(A',Z)$ cancel most of that background and isolate $\delta\langle r^2\rangle$. Electron scattering and muonic atoms calibrate the absolute scale that isotope shifts then track along a chain.

## 1.11 Physics depth: finite-size energy and isotope differences

A pointlike nucleus would produce hydrogenic energies fixed by $Z$ and reduced mass alone. Finite size spreads the proton charge over a ball of radius $\sim R$, lowering the electrostatic potential felt by an $s$-electron (or muon) inside the nucleus and shifting level energies.

### 1.11.1 Worked estimate: $1s$ shift scaling

In first-order perturbation theory the leading finite-size correction scales as

$$\Delta E_{1s} \propto Z^4 \langle r^2 \rangle |\psi(0)|^2, \tag{1.51}$$

with $|\psi(0)|^2$ enormous for muonic atoms because $m_\mu/m_e \simeq 207$ shrinks the Bohr radius. For ordinary electronic $K_\alpha$ shifts the effect is parts in $10^4$ or smaller; for muonic X-rays it reaches mega-electronvolt scales in heavy elements. Isotope shifts cancel most atomic-structure background and leave $\delta\langle r^2 \rangle$ as the nuclear observable.

**King-plot linearity intuition**

Two optical transitions with field-shift factors $F_i$ and mass-shift coefficients $K_i$ give a linear King plot if only the leading $\langle r^2 \rangle$ and mass terms matter. Curvature signals either higher nuclear moments (deformation, polarisability) or an incomplete electronic factor. Before claiming new physics, vary $F$ within published uncertainties and recompute the residual.

**Remark**

**Limits.** Optical isotope shifts are differential; electron scattering and muonic atoms set the absolute radius ladder. Mixing the two without a common radius convention (point vs rms vs diffraction) produces apparent discrepancies that are only definitional.

### 1.11.2 Muonic versus electronic leverage

The muonic Bohr radius scales as $1/(Zm_\mu)$. For lead, the muon $1s$ wave function has substantial overlap with the nuclear volume, so the finite-size shift is a leading, not perturbative, piece of the X-ray energy. Electronic isotope shifts reverse the hierarchy: the nuclear piece is a small correction on top of a huge atomic transition, which is why differential measurements and King plots are essential.

Deformation adds a quadrupole contribution to $\langle r^2 \rangle$ and can produce odd–even staggering beyond simple pairing. When an isotopic chain crosses a shape transition (Lecture 15), the slope of $\langle r^2 \rangle$ versus $N$ changes abruptly. Charge radii are therefore collective as well as single-particle observables.

Practical analysis often quotes the Barrett radius or a Fourier-Bessel fit rather than a single rms number. When converting a published isotope shift into $\delta\langle r^2 \rangle$, write the field-shift formula with units and the electronic factor $F$ explicitly, then propagate $\delta F$. A 10% error in $F$ is common and can dominate the nuclear uncertainty budget for light chains where the field shift is not overwhelming.

#### Worked optical versus muonic comparison

Take a published optical $\delta\langle r^2 \rangle$ along even–even cadmium or tin and convert to a differential radius. Compare the absolute radius at the anchor isotope with a muonic or elastic-electron value. Discrepancies at the 0.01 fm level are common and usually reflect electronic-factor or

model-radius definitions rather than a failure of finite-size theory. Document definitions beside every number.

**Physics-depth close**

Isotope shifts are differential nuclear radii dressed in atomic clothing. The nuclear content is $\delta\langle r^2\rangle$; the atomic content is $F$ and $K$. Separating them cleanly is the craft this chapter adds to the absolute form-factor programme of Lecture 1.

## 1.12 Further physics: separation energies and the isotope-shift ladder

Atomic size enters spectroscopy through level shifts; nuclear size also leaves fingerprints in the energies needed to remove a nucleon. The neutron and proton separation energies

$$S_n = \big[M(A-1,Z)+m_n-M(A,Z)\big]c^2, \qquad S_p = \big[M(A-1,Z-1)+m(^1\mathrm{H})-M(A,Z)\big]c^2 \tag{1.52}$$

are the nuclear analogues of ionisation energies: they probe valence nucleons. Sharp jumps in $S_n$ or $S_p$ at closed shells are shell signatures; smooth trends with $A$ and $Z$ follow the SEMF surface, Coulomb, and pairing terms (Lectures 4–5) [13, 6, 1].

Finite-size shifts of $s$ levels and separation-energy systematics are complementary: both are sensitive to how tightly the outer nucleons (or the electron cloud near $r = 0$) feel the nuclear interior.

### 1.12.1 Mirror nuclei and a Coulomb-radius estimate

Binding-energy differences of mirror pairs provide an independent size check. For example,

$$B(^3\mathrm{H}) - B(^3\mathrm{He}) \approx 0.76\,\mathrm{MeV}$$

is largely the Coulomb energy of the two protons in $^3$He. Writing

$$\Delta B \approx \frac{e^2}{4\pi\varepsilon_0}\Big\langle\frac{1}{r_{12}}\Big\rangle \sim \frac{e^2}{4\pi\varepsilon_0 R}$$

yields $R \sim 2\,\mathrm{fm}$, consistent with other light-nucleus radii [14]. Finite-size isotope shifts (this lecture) and mirror Coulomb differences are two faces of the same electrostatic physics.

### 1.12.2 Isotope-shift ladder: optical, $K_\alpha$, and muonic

Three experimental ladders measure the same change of nuclear mean-square radius between isotopes $A$ and $A'$ [6, 1]:

1. **Optical isotope shifts** (valence transitions). The electron density at the nucleus is small, so shifts are tiny (parts in $10^6$ of optical frequencies) but laser spectroscopy resolves them for long chains of radioactive isotopes.

2. $K_\alpha$ **X-ray isotope shifts.** The $2p \to 1s$ transition energy difference between isotopes is essentially the difference of $1s$ finite-size shifts, because $p$ wave functions vanish at $r = 0$. A plot of $\Delta E_K$ versus $A^{2/3}$ is approximately linear for a sequence of isotopes [6].

3. **Muonic X rays.** The muon Bohr radius is $\sim m_e/m_\mu$ times smaller than the electronic one, so the muon spends a much larger fraction of its time inside the nucleus. Isotope shifts are correspondingly huge and dominate over many atomic-structure uncertainties.

For a uniform sphere the first-order $1s$ finite-size shift scales as

$$\Delta E_{1s} \propto Z\,|\psi_{1s}(0)|^2\,\langle r^2\rangle_{\rm ch} \propto Z^4 R^2, \tag{1.53}$$

so $\Delta E(A) - \Delta E(A') \propto R^2(A) - R^2(A')$. All three methods, after careful atomic-structure corrections, return $R_0$ consistent with electron scattering ($\sim 1.2\,\mathrm{fm}$).

### 1.12.3 Forward look: magic numbers in separation energies

Just as atomic ionisation energies jump at noble-gas $Z$, nuclear separation energies jump at magic $N$ or $Z$:

$$N, Z = 2, 8, 20, 28, 50, 82, 126. \tag{1.54}$$

Lead isotopes show a clear discontinuity in $S_n$ at $N = 126$ ($^{208}$Pb). The SEMF alone is smooth; the excess binding of magic and doubly magic nuclei relative to the liquid-drop fit is a shell-model signature that returns when single-particle potentials are discussed [14, 6]. For now it is enough that size probes and separation energies both organise the chart of nuclides before binding-energy systematics take over in Lecture 4.

## 1.13 Deeper reading: from $\langle r^2\rangle$ to the nuclear chart

Along an isotopic chain, $\langle r^2\rangle$ generally grows with $N$, but shell closures and deformation onsets produce slope changes and odd–even staggering. Those features are the spectroscopic fingerprints that Lectures 12–15 will reinterpret with single-particle and collective language.

### 1.13.1 Order-of-magnitude bridge

A change $\delta\langle r^2\rangle = 0.1\,\mathrm{fm}^2$ is a sub-percent effect on $R_{\rm rms} \sim 5\,\mathrm{fm}$, yet it is routinely resolved by laser spectroscopy. That sensitivity is why radioactive-beam isotope-shift programmes map charge radii far from stability where electron-scattering form factors are inaccessible. Lecture 1 still supplies the absolute calibration; Lecture 3 supplies the differential microscope; Lecture 5's mass parabolas ask a parallel question for binding rather than size.

### 1.13.2 Field shift versus mass shift

The mass shift contains normal and specific contributions from electron correlations. In light nuclei the mass shift can dominate; in heavy nuclei the field shift wins. Separating them requires either a King plot with two transitions or ab initio electronic factors. Nuclear physicists consuming isotope-shift radii should always ask which electronic factors were used and whether

a King-plot nonlinearity was tested. That discipline prevents over-interpreting a radius kink as a shell closure when it might be an electronic-structure artefact.

Practical analysis often quotes the Barrett radius or a Fourier-Bessel fit rather than a single rms number. When converting a published isotope shift into $\delta\langle r^2\rangle$, write the field-shift formula with units and the electronic factor $F$ explicitly, then propagate $\delta F$. A 10% error in $F$ is common and can dominate the nuclear uncertainty budget for light chains where the field shift is not overwhelming.

### Isotope-shift checklist

Write $\delta\nu = F\,\delta\langle r^2\rangle + K\,\mu$ (schematic) with units, cite the electronic factor source, and test King-plot linearity for two transitions. If nonlinearity remains after varying $F$ within uncertainties, only then consider higher nuclear moments or speculative new interactions. Tie absolute anchors to muonic or electron-scattering radii so that a beautiful differential chain does not float in absolute scale.

### Odd-even staggering and deformation

Odd–even staggering in charge radii often tracks pairing and the blocking of deformation. A sudden onset of deformation produces a kink in $\langle r^2\rangle(N)$ larger than any smooth liquid-drop expectation. Comparing radius kinks with $E(2^+)$ systematics (Lecture 15) is the standard way to decide whether a kink is a shell closure or a shape change.

### Muonic ladder

Muonic X-ray cascades provide absolute radii for stable and long-lived targets that optical methods then use as anchors. When an optical chain is attached to a muonic absolute radius at one isotope, residual electronic-factor errors still affect isotope differences, but the absolute float is reduced. Document the anchor isotope explicitly in any radius table you compile.

### Definition hygiene

Make a three-column table for one nucleus: point radius, rms radius, and diffraction radius, with references. The spreads are educational. Isotope-shift papers must state which electronic factors convert frequencies into $\delta\langle r^2\rangle$; copy those citations into your notes whenever you adopt a radius value for structure comparisons in later chapters.

Finite-size physics is therefore a conversion problem: electronic or muonic probes supply energies, nuclear models supply moments of charge, and the shared language is $\langle r^2\rangle$ and its isotopic differences. Mastering that conversion is the practical skill Lecture 3 adds to Lecture 1's form factors.

In practice, rework one numerical estimate from the lecture with a different parameter set and compare the shift to the quoted experimental uncertainty. If the shift exceeds the uncertainty, the estimate is teaching a scale, not delivering a fit. That distinction keeps theoretical cartoons honest when they sit beside evaluated data tables and modern many-body calculations. Along the course arc, write one sentence linking this chapter backward and one forward: the discipline

of those two sentences is as important as any single formula. Examination problems rarely ask for a literature review, but they do ask for the scale argument that literature reviews presuppose.

**Research frontier: isotope shifts, King plots, and student projects**

Finite-size corrections and isotope-shift ideas of Lecture 3 are now precision tools that sit at the border of atomic, nuclear, and particle physics. Modern laser and ion-trap spectroscopy measures optical isotope shifts at the hundred-hertz level; King plots of two transitions test the linearity expected from a simple field-plus-mass decomposition. Nonlinearities have been reported in $Yb^+$ and can arise either from higher-order nuclear structure (including deformation and nuclear polarisability) or from a hypothetical light boson mediating a new force between electrons and neutrons, so nuclear and particle interpretations must be disentangled carefully [55]. Evaluated charge-radius compilations remain the nuclear input for such analyses [56]. Muonic-atom X-rays continue to provide absolute size anchors for stable and long-lived species, while radioactive-molecule spectroscopy and trapped radioactive ions extend electroweak and size sensitivity at rare-isotope facilities [52]. Uncertainties that still dominate many King-plot interpretations include electronic factors $F$, specific mass-shift calculations, and incomplete knowledge of nuclear deformation along isotopic chains.

For nuclear-physics students, the practical skill is to separate electronic structure uncertainties from nuclear size uncertainties before claiming new physics. A careful King-plot analysis therefore begins with evaluated radii and documented electronic factors, then tests whether residual nonlinearities survive when nuclear deformation and higher-order field shifts are varied within published ranges.

*Student directions.* (1) Data project: construct a King plot from two published isotope-shift tables and fit the linear slope. (2) Analytic estimate: estimate $\delta\langle r^2\rangle$ from a measured field shift using a textbook electronic factor $F$. (3) Literature comparison: compare optical and muonic determinations of $\langle r^2\rangle$ for one even-even chain and discuss residual model dependence.

## 1.14 Problems with solutions

**Problem 3.1 — Finite-size shift for a uniform sphere**

Show that for a hydrogen-like $1s$ electron and a uniform nuclear charge of radius $R \ll a_0/Z$, the first-order energy shift relative to a point nucleus is

$$\Delta E \approx \frac{2}{5}\frac{Z^4 e^2}{4\pi\varepsilon_0}\frac{R^2}{a_0^3}$$

(up to the standard hydrogenic normalisation constants; cf. Krane §3.1). Estimate $\Delta E$ for $Z = 80$, $R = 7\,\mathrm{fm}$.

**Solution 3.1**

Inside a uniform sphere the potential energy of an electron is

$$U_{\text{finite}}(r) = -\frac{Ze^2}{8\pi\varepsilon_0 R}\left(3 - \frac{r^2}{R^2}\right), \qquad r \le R,$$

while $U_{\text{point}} = -Ze^2/(4\pi\varepsilon_0 r)$. Their difference $H_1$ vanishes for $r > R$. With $|\psi_{1s}(0)|^2 = Z^3/(\pi a_0^3)$ nearly constant over the nucleus,

$$\int_{r<R} H_1 \, \mathrm{d}^3 r = \frac{2\pi}{5}\,\frac{Ze^2}{4\pi\varepsilon_0}\,R^2,$$

$$\Delta E = |\psi(0)|^2 \int H_1 \, \mathrm{d}^3 r = \frac{2}{5}\,\frac{Z^4 e^2}{4\pi\varepsilon_0}\,\frac{R^2}{a_0^3}.$$

(The factor 2/5 is the uniform-sphere special case of the $\langle r^2\rangle = \frac{3}{5}R^2$ theorem.) For $Z = 80$, $R = 7\,\text{fm} = 7 \times 10^{-15}\,\text{m}$, $a_0 = 5.29 \times 10^{-11}\,\text{m}$,

$$\frac{R^2}{a_0^3} \approx 3.3 \times 10^{-22}\,\text{m}^{-1}, \qquad \Delta E \approx 7.8\,\text{eV}$$

using $e^2/(4\pi\varepsilon_0) = 1.440\,\text{MeV fm}$. This is small on a $K$-shell scale of tens of keV, but isotope *differences* are measurable. The non-relativistic estimate is not a precision result at $Z = 80$.

**Problem 3.2 — Isotope shift and $A^{1/3}$**

Two isotopes of the same element have mass numbers $A$ and $A'$ and radii $R = r_0 A^{1/3}$, $R' = r_0 (A')^{1/3}$. Argue that the difference of finite-size $1s$ shifts scales as

$$\Delta E(A) - \Delta E(A') \propto Z^4 (A^{2/3} - A'^{2/3}).$$

Why is a plot of $K_\alpha$ X-ray isotope shifts versus $A^{2/3}$ expected to be approximately linear?

**Solution 3.2**

From Problem 3.1, $\Delta E \propto Z^4 R^2$ and $R^2 \propto A^{2/3}$. Hence

$$\delta(\Delta E) \propto Z^4 (A^{2/3} - A'^{2/3}).$$

Plotting measured isotope shifts against $A^{2/3}$ (relative to a reference isotope) should be nearly linear with slope fixed by $r_0$. Deviations encode shell effects and deformation [6].

**Problem 3.3 — Muonic enhancement**

By what factor does the finite-size shift grow if the electron is replaced by a muon ($m_\mu/m_e \approx 207$), all else equal?

**Solution 3.3**

The Bohr radius scales as $1/\mu$, and $|\psi(0)|^2 \propto 1/a^3 \propto \mu^3$. Replacing $m_e$ by $m_\mu$ therefore multiplies $\Delta E$ by

$$\Delta E_\mu = \left(\frac{m_\mu}{m_e}\right)^3 \Delta E_e \approx 207^3 \Delta E_e = 8.86 \times 10^6 \, \Delta E_e \sim 9 \times 10^6 \, \Delta E_e.$$

Caveat: for heavy nuclei the muon $1s$ orbit has size comparable to $R$, so the constant-$\psi(0)$ approximation and non-relativistic theory both need upgrading; the factor $\sim 10^7$ is the scaling estimate, not a precision prediction. Muonic $K_\alpha$ X-rays are a nuclear-size measurement, not an atomic one.

# Bibliography


[1] R. A. Dunlap, *An Introduction to the Physics of Nuclei and Particles* (2nd ed.), IOP Publishing, Bristol (2023), DOI: 10.1088/978-0-7503-6094-4, Ch. 3 (Nuclear composition and size).

[2] W. Demtröder, *Nuclear and Particle Physics*, Undergraduate Lecture Notes in Physics, Springer, Cham (2023).

[3] S. Petrera, *Problems and Solutions in Nuclear and Particle Physics*, UNITEXT for Physics, Springer, Cham (2019).

[4] F. Terranova, *A Modern Primer in Particle and Nuclear Physics*, Oxford University Press (2021).

[5] S. D'Auria, *Introduction to Nuclear and Particle Physics*, Undergraduate Lecture Notes in Physics, Springer, Cham (2018).

[6] K. S. Krane, *Introductory Nuclear Physics*, Wiley, New York (1988).

[7] R. Hofstadter, "Electron scattering and nuclear structure," Rev. Mod. Phys. **28**, 214 (1956).

[8] H. F. Ehrenberg, R. Hofstadter, U. Meyer-Berkhout, D. G. Ravenhall, and S. E. Sobottka, "High-Energy Electron Scattering and the Charge Distribution of Carbon-12 and Oxygen-16," Phys. Rev. **113**, 666 (1959).

[9] H. Yukawa, "On the interaction of elementary particles. I," Proc. Phys.-Math. Soc. Japan **17**, 48 (1935).

[10] R. D. Woods and D. S. Saxon, "Diffuse surface optical model for nucleon-nuclei scattering," Phys. Rev. **95**, 577 (1954).

[11] H. G. J. Moseley, "The high-frequency spectra of the elements," Phil. Mag. **26**, 1024 (1913); **27**, 703 (1914).

[12] C. F. von Weizsäcker, "Zur Theorie der Kernmassen," Z. Phys. **96**, 431 (1935).

[13] P. Cappellaro, *Introduction to Applied Nuclear Physics* (MIT OpenCourseWare / LibreTexts), CC BY-NC-SA 4.0.

[14] J.-L. Basdevant, J. Rich, and M. Spiro, *Fundamentals in Nuclear Physics: From Nuclear Structure to Cosmology*, Springer, New York (2005).

[15] D. Tong, *Particle Physics*, Lecture notes (University of Cambridge / CERN school notes).

[16] M. G. Mayer, "On closed shells in nuclei. II," Phys. Rev. **75**, 1969 (1949).

[17] O. Haxel, J. H. D. Jensen, and H. E. Suess, "On the "magic numbers" in nuclear structure," Phys. Rev. **75**, 1766 (1949).

[18] T. Schmidt, "Über die magnetischen Momente der Atomkerne," Z. Phys. **106**, 358 (1937).

[19] L. W. Nordheim, "On spins, moments, and shells in nuclei," Phys. Rev. **78**, 294 (1950).

[20] Evaluated Nuclear Structure Data File (ENSDF), National Nuclear Data Center, Brookhaven National Laboratory, `https://www.nndc.bnl.gov/ensdf/`.

[21] NuDat 3, National Nuclear Data Center, Brookhaven National Laboratory, `https://www.nndc.bnl.gov/nudat3/`.

[22] N. J. Stone, "Table of nuclear magnetic dipole and electric quadrupole moments," At. Data Nucl. Data Tables **90**, 75 (2005); updated compilations at NNDC.

[23] W. N. Cottingham and D. A. Greenwood, *An Introduction to Nuclear Physics* (2nd ed.), Cambridge University Press, Cambridge (2001).

[24] H. Geiger and J. M. Nuttall, "The ranges of the $\alpha$ particles from the radioactive substances," Phil. Mag. **22**, 613 (1911).

[25] G. Gamow, "Zur Quantentheorie des Atomkernes," Z. Phys. **51**, 204 (1928).

[26] R. W. Gurney and E. U. Condon, "Wave mechanics and radioactive disintegration," Nature **122**, 439 (1928); Phys. Rev. **33**, 127 (1929).

[27] M. Wang, W. J. Huang, F. G. Kondev, G. Audi, and S. Naimi, "The AME 2020 atomic mass evaluation (II). Tables, graphs and references," Chin. Phys. C **45**, 030003 (2021).

[28] Laboratoire National Henri Becquerel (LNHB), Recommended decay data, `http://www.lnhb.fr/nuclear-data/nuclear-data-table/`.

[29] L. M. Langer, R. D. Moffat, and H. C. Price, Jr., "Low energy beta-ray spectra: $P^{32}$ and $Cu^{64}$," Phys. Rev. **76**, 1725 (1949).

[30] L. M. Langer and H. C. Price, Jr., "Shapes of the beta-spectra of the forbidden transitions of $Sb^{124}$, $Rb^{86}$, $Sr^{89}$, $Y^{91}$, and $Cs^{137}$," Phys. Rev. **75**, 1769 (1949).

[31] D. C. Camp and L. M. Langer, "The shape of the $^{66}$Ga positron spectrum and the contribution from $0^+ \to 0^+$ transitions," Phys. Rev. **129**, 1782 (1963).

[32] H. C. Verma, *Nuclear Physics: Fundamentals and Applications*, NPTEL/IIT Kanpur lecture series, `https://hcverma.in/ncl_phy_lectures`.

[33] International Atomic Energy Agency, *LiveChart of Nuclides*, evaluated structure, decay, reaction, and fission-yield data, `https://www-nds.iaea.org/relnsd/vcharthtml/VChartHTML.html`.

[34] T. Kibédi, T. W. Burrows, M. B. Trzhaskovskaya, P. M. Davidson, and C. W. Nestor, Jr., "Evaluation of theoretical conversion coefficients using BrIcc," Nucl. Instrum. Methods Phys. Res. A **589**, 202 (2008), DOI: 10.1016/j.nima.2008.02.051.

[35] D. A. Brown *et al.*, "ENDF/B-VIII.0: The 8th major release of the nuclear reaction data library with CIELO-project cross sections, new standards and thermal scattering data," Nucl. Data Sheets **148**, 1 (2018), DOI: 10.1016/j.nds.2018.02.001.

[36] B. Acharya *et al.*, "Solar fusion III: New data and theory for hydrogen-burning stars," Rev. Mod. Phys. **97**, 035002 (2025), DOI: 10.1103/8lm7-gs18.

[37] S. N. Ghoshal, "An experimental verification of the theory of compound nucleus," Phys. Rev. **80**, 939 (1950), DOI: 10.1103/PhysRev.80.939.

[38] D. Adhikari *et al.* (PREX Collaboration), "Accurate determination of the neutron skin thickness of $^{208}$Pb through parity-violation in electron scattering," Phys. Rev. Lett. **126**, 172502 (2021), DOI: 10.1103/PhysRevLett.126.172502.

[39] B. T. Reed, F. J. Fattoyev, C. J. Horowitz, and J. Piekarewicz, "Implications of PREX-II on the equation of state of neutron-rich matter," Phys. Rev. Lett. **126**, 172503 (2021), DOI: 10.1103/PhysRevLett.126.172503.

[40] B. Hu *et al.*, "Ab initio predictions link the neutron skin of $^{208}$Pb to nuclear forces," Nature Phys. **18**, 1196 (2022), DOI: 10.1038/s41567-022-01715-8.

[41] E. Epelbaum, H.-W. Hammer, and U.-G. Meißner, "Modern theory of nuclear forces," Rev. Mod. Phys. **81**, 1773 (2009), DOI: 10.1103/RevModPhys.81.1773.

[42] H.-W. Hammer, S. König, and U. van Kolck, "Nuclear effective field theory: Status and perspectives," Rev. Mod. Phys. **92**, 025004 (2020), DOI: 10.1103/RevModPhys.92.025004.

[43] T. Otsuka, A. Gade, O. Sorlin, T. Suzuki, and Y. Utsuno, "Evolution of shell structure in exotic nuclei," Rev. Mod. Phys. **92**, 015002 (2020), DOI: 10.1103/RevModPhys.92.015002.

[44] H. Hergert, S. K. Bogner, T. D. Morris, A. Schwenk, and K. Tsukiyama, "The in-medium similarity renormalization group: A novel ab initio method for nuclei," Phys. Rep. **621**, 165 (2016), DOI: 10.1016/j.physrep.2015.12.007.

[45] J. M. Lattimer and M. Prakash, "The equation of state of hot, dense matter and neutron stars," Phys. Rep. **621**, 127 (2016), DOI: 10.1016/j.physrep.2015.12.005.

[46] J. M. Lattimer, "Neutron stars and the nuclear matter equation of state," Annu. Rev. Nucl. Part. Sci. **71**, 433 (2021), DOI: 10.1146/annurev-nucl-102419-124827.

[47] B. P. Abbott *et al.* (LIGO Scientific Collaboration and Virgo Collaboration), "GW170817: Observation of gravitational waves from a binary neutron star inspiral," Phys. Rev. Lett. **119**, 161101 (2017), DOI: 10.1103/PhysRevLett.119.161101.

[48] M. J. Dolinski, A. W. P. Poon, and W. Rodejohann, "Neutrinoless double-beta decay: Status and prospects," Annu. Rev. Nucl. Part. Sci. **69**, 219 (2019), DOI: 10.1146/annurev-nucl-101918-023407.

[49] M. Agostini, G. Benato, J. A. Detwiler, J. Menéndez, and F. Vissani, "Toward the discovery of matter creation with neutrinoless $\beta\beta$ decay," Rev. Mod. Phys. **95**, 025002 (2023), DOI: 10.1103/RevModPhys.95.025002.

[50] P. Gysbers *et al.*, "Discrepancy between experimental and theoretical $\beta$-decay rates resolved from first principles," Nature Phys. **15**, 428 (2019), DOI: 10.1038/s41567-019-0450-7.

[51] H. L. Crawford, K. Fossez, S. König, and A. Spyrou, "A vision for the science of rare isotopes," Annu. Rev. Nucl. Part. Sci. **74**, 141 (2024), DOI: 10.1146/annurev-nucl-121423-091501.

[52] Nuclear Science Advisory Committee, *A New Era of Discovery: The 2023 Long Range Plan for Nuclear Science*, U.S. Department of Energy and National Science Foundation (2023), `https://nuclearsciencefuture.org/`.

[53] S. A. Giuliani, Z. Matheson, W. Nazarewicz, E. Olsen, P.-G. Reinhard, J. Sadhukhan, B. Schuetrumpf, N. Schunck, and P. Schwerdtfeger, "Colloquium: Superheavy elements: Oganesson and beyond," Rev. Mod. Phys. **91**, 011001 (2019), DOI: 10.1103/RevModPhys.91.011001.

[54] N. Schunck and D. Regnier, "Theory of nuclear fission," Prog. Part. Nucl. Phys. **125**, 103963 (2022), DOI: 10.1016/j.ppnp.2022.103963.

[55] I. Counts, J. Hur, D. P. L. Aude Craik, H. Jeon, C. Leung, J. C. Berengut, A. Geddes, A. Kawasaki, W. Jhe, and V. Vuletić, "Evidence for nonlinear isotope shift in $Yb^+$ search for new boson," Phys. Rev. Lett. **125**, 123002 (2020), DOI: 10.1103/PhysRevLett.125.123002.

[56] I. Angeli and K. P. Marinova, "Table of experimental nuclear ground state charge radii: An update," At. Data Nucl. Data Tables **99**, 69 (2013), DOI: 10.1016/j.adt.2011.12.006.

[57] S. Kraemer *et al.*, "Observation of the radiative decay of the $^{229}$Th nuclear clock isomer," Nature **617**, 706 (2023), DOI: 10.1038/s41586-023-05894-z.